ResearchGate

See discussions, stats, and author profiles for this publication at: https://www.researchgate.net/publication/51773685

Visible-light photocurrent response of TiO2-polyheptazine hybrids: Evidence for interfacial charge-transfer absorption

ARTICLE *in* PHYSICAL CHEMISTRY CHEMICAL PHYSICS · NOVEMBER 2011

Impact Factor: 4.49 · DOI: 10.1039/c1cp22861g · Source: PubMed

CITATIONS
32

READS
96

10 AUTHORS, INCLUDING:

Oleksiy V. Khavryuchenko
40 PUBLICATIONS **184** CITATIONS
SEE PROFILE

Volodymyr Khavryuchenko
18 PUBLICATIONS **98** CITATIONS
SEE PROFILE

Jennifer Strunk
Max Planck Institute for Chemical Energy C…
49 PUBLICATIONS **750** CITATIONS
SEE PROFILE

Radim Beranek
Universität Ulm
34 PUBLICATIONS **1,089** CITATIONS
SEE PROFILE

Available from: Radim Beranek
Retrieved on: 26 January 2016

PCCP

Dynamic Article Links

Cite this: *Phys. Chem. Chem. Phys.*, 2011, **13**, 21511–21519

www.rsc.org/pccp

PAPER

Visible-light photocurrent response of TiO_2–polyheptazine hybrids: evidence for interfacial charge-transfer absorption†

Michal Bledowski,‡[a] Lidong Wang,‡[a] Ayyappan Ramakrishnan,[a] Oleksiy V. Khavryuchenko,[b] Volodymyr D. Khavryuchenko,[c] P. Carlo Ricci,[d] Jennifer Strunk,[e] Till Cremer,[f] Claudia Kolbeck[f] and Radim Beranek*[ag]

Received 8th September 2011, Accepted 12th October 2011
DOI: 10.1039/c1cp22861g

We investigated photoelectrodes based on TiO_2–polyheptazine hybrid materials. Since both TiO_2 and polyheptazine are extremely chemically stable, these materials are highly promising candidates for fabrication of photoanodes for water photooxidation. The properties of the hybrids were experimentally determined by a careful analysis of optical absorption spectra, luminescence properties and photoelectrochemical measurements, and corroborated by quantum chemical calculations. We provide for the first time clear experimental evidence for the formation of an interfacial charge-transfer complex between polyheptazine (donor) and TiO_2 (acceptor), which is responsible for a significant red shift of absorption and photocurrent response of the hybrid as compared to both of the single components. The direct optical charge transfer from the HOMO of polyheptazine to the conduction band edge of TiO_2 gives rise to an absorption band centered at 2.3 eV (540 nm). The estimated potential of photogenerated holes (+1.7 V *vs.* NHE, pH 7) allows for photooxidation of water (+0.82 V *vs.* NHE, pH 7) as evidenced by visible light-driven ($\lambda > 420$ nm) evolution of dioxygen on hybrid electrodes modified with IrO_2 nanoparticles as a co-catalyst. The quantum-chemical simulations demonstrate that the TiO_2–polyheptazine interface is a complex and flexible system energetically favorable for proton-transfer processes required for water oxidation. Apart from water splitting, this type of hybrid materials may also find further applications in a broader research area of solar energy conversion and photo-responsive devices.

Introduction

The development of artificial photochemical systems capable of mimicking natural photosynthesis has attracted significant interest motivated by the need to secure the future supply of clean and sustainable energy.[1–3] Among other strategies, research has focused on novel types of semiconductor-based photocatalysts allowing for solar energy to be captured, converted and directly stored in high-energy chemical bonds of hydrogen molecules produced by water splitting. The photocatalytic water-splitting systems can be designed in several ways.[4,5] In the simplest approach, the photocatalyst is employed in the form of a powder suspension whereby both water splitting reactions—oxygen evolution and hydrogen evolution—occur at the same particle.[6–9] Alternatively, the water oxidation and reduction reactions can be spatially separated by implementing the photocatalyst into a photoelectrode in a photoelectrochemical cell.[10–12] Due to their inherent constructional and functional simplicity, these *photochemical* approaches are potentially more efficient and cheaper than direct water splitting using an electrolyzer driven by a conventional photovoltaic cell array. Importantly, it is the water *oxidation* reaction which is the real ''bottleneck'' of any water-splitting device.[13] This is because—in contrast to the two-electron hydrogen evolution reaction that is mechanistically relatively simple—the oxygen-evolving reaction is a highly complex process requiring proton-coupled transfer of four

[a] *Inorganic Chemistry II, Faculty of Chemistry and Biochemistry, Ruhr University Bochum, Universitätstr. 150, D-44780 Bochum, Germany. E-mail: radim.beranek@rub.de; Fax: +49-234-3214174; Tel: +49-234-3229431*
[b] *Department of Chemistry, Kyiv National Taras Shevchenko University, Volodymyrska Str. 64, UA-01033, Kyiv, Ukraine*
[c] *Institute for Sorption and Problems of Endoecology, National Academy of Sciences of Ukraine, 13 General Naumov Str., UA-03167 Kyiv, Ukraine*
[d] *Dipartimento di Fisica, Università di Cagliari, s.provinciale Monserrato-Sestu Km 0,700, 09042 Monserrato, Cagliari, Italy*
[e] *Industrial Chemistry, Faculty of Chemistry and Biochemistry, Ruhr University Bochum, Universitätstr. 150, D-44780 Bochum, Germany*
[f] *Physical Chemistry II, Department of Chemistry and Pharmacy, University of Erlangen-Nuremberg, Egerlandstr. 3, D-91058 Erlangen, Germany*
[g] *Materials Research Department, Ruhr University Bochum, D-44801 Bochum, Germany*

† Electronic supplementary information (ESI) available: XRD, Raman, PL, XP, and optical absorption spectra; calculated enthalpy of formation for different deformations of PH5 cluster; figure of Ti54M1-H-amide cluster; potential dependence of photocurrent. See DOI: 10.1039/c1cp22861g

‡ These authors contributed equally to this work.

electrons from two water molecules.[14–17] This often translates into slow kinetics and considerable overpotentials required for efficient oxygen evolution.[18]

Accordingly, one of the fundamental challenges in photoelectrochemical water splitting is the development of highly efficient and stable photoanodes with suitable optical (bandgap), photoelectrochemical (position of band edges on the energy scale), and surface catalytic properties.[12,19] The complexity of this task is well illustrated by the manifold attempts to utilize metal oxide materials like TiO_2, WO_3, and Fe_2O_3.[5,20–29] These n-type semiconductors are very attractive due to their high chemical stability and relative abundance in nature. However, none of them possesses *both* the bandgap low enough to absorb a significant portion of visible light *and* the potential of the conduction band edge negative enough to allow for proton reduction without the need to apply additional electric bias (Fig. 1).[12,19,30] The success of photochemical approaches to water splitting therefore depends utterly on our ability to synthesize *new* robust materials with well-tailored optical and photoelectrochemical properties.[31]

The search for suitable photoanodes currently involves a great variety of diverse approaches including structural and surface engineering of pristine low-bandgap semiconductors (like, *e.g.*, Fe_2O_3, WO_3, or $BiVO_4$),[25,32,33] synthesis of doped and mixed-metal oxides using high-throughput combinatorial protocols,[34–37] or sensitization of nanocrystalline TiO_2 electrodes by ruthenium dye molecules coupled to a colloidal $IrO_2{\cdot}nH_2O$ oxygen evolving catalyst.[38]

Recently, one of us (R. B.) developed a novel type of visible-light active photoelectrodes based on materials consisting of titanium dioxide modified at the surface with an organic compound containing nitrogen and carbon (Fig. 2a).[39–41] Such electrodes exhibited significant visible-light induced anodic photocurrents. The intensely yellow materials can be prepared, for example, by simply heating TiO_2 in a gaseous atmosphere of urea pyrolysis products.[39–41] The chemistry behind the modification procedure was elucidated by Mitoraj and Kisch[42,43] who identified the nitrogen and carbon-containing species as poly(tri-*s*-triazine) (polyheptazine) formed *in situ* at the surface of titania from urea pyrolysis products (Fig. 2b). Interestingly, polyheptazine-type compounds belong to the oldest polymers ever synthesized. They were first prepared by Berzelius in 1830, and few years later, due to their yellowish color, coined as "melon" by Liebig.[44] The polyheptazine sheets represent a highly stable delocalized system of conjugated π-bonds and form graphite-like structures through π-πstacking with a stacking distance of 0.325 nm (see ESI†, Fig. S1). Notably, *pristine*

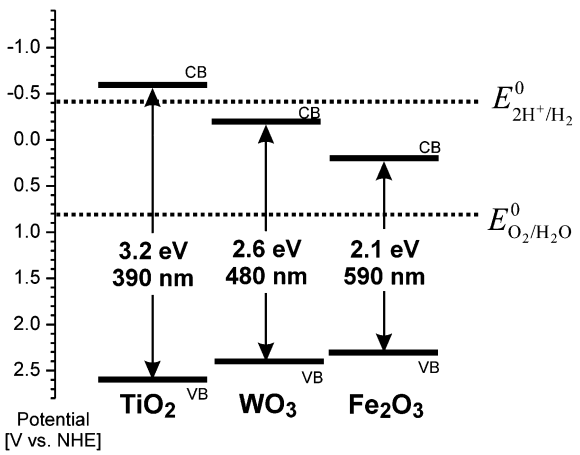

Fig. 1 The potentials of the conduction (CB) and valence band (VB) edges of anatase TiO_2, monoclinic WO_3, and α-Fe_2O_3 at pH 7. The reduction potential of water (−0.41 V *vs.* NHE at pH 7) is more negative than the conduction band edge of WO_3 and Fe_2O_3, which would require an additional electric bias applied in order to allow for water reduction at the counter electrode. The electrochemical potential of electrons photogenerated in TiO_2 is potentially negative enough to reduce protons. However, the large bandgap of anatase (3.2 eV) enables absorption only in the UV region, a tiny part (3–4%) of the solar spectrum.

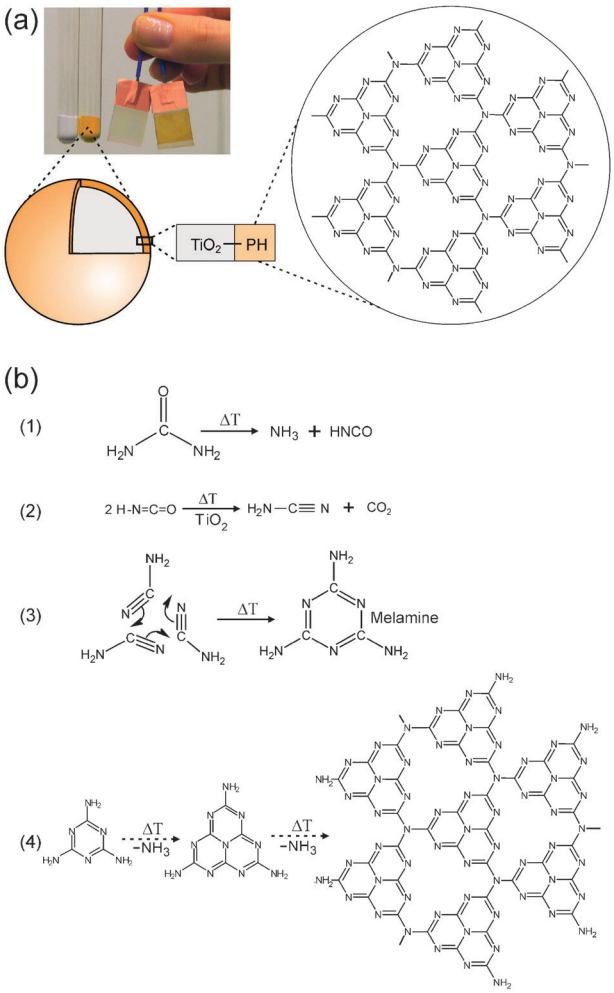

Fig. 2 (a) Photograph of pristine anatase TiO_2 (white) and TiO_2–polyheptazine hybrid materials (yellow) with a simplified view of TiO_2 modified at the surface by polyheptazine. (b) A sequence of reactions leading to formation of polyheptazine from urea at elevated temperatures (300–500 °C):[42,43] urea decomposes predominantly to ammonia and isocyanic acid (eqn (1)); titania catalyzes conversion of isocyanic acid into cyanamide (eqn (2)) which, in turn, trimerizes to form melamine (2,4,6-triamino-*s*-triazine) (eqn (3));[49,50] melamine then undergoes condensation to 2,5,8-triamino-tri-*s*-triazine (*s*-heptazine) and further to extended polyheptazine networks (eqn (4)).[51–57] The precise structure of polyheptazine sheets is currently under intense investigations (see particularly the recent work of Schnick *et al.*[58,59]).

This journal is © the Owner Societies 2011

polyheptazine-type powders, designated as "graphitic carbon nitride", were recently introduced as visible-light active photocatalysts by X. Wang *et al*. and their photoactivity is now being intensely investigated.[45–48]

We currently investigate *hybrid* materials consisting of TiO_2 covered by polyheptazine, particularly in view of utilizing these unique materials in efficient photoanodes for water oxidation. One of the most exciting features of these materials is their intense visible light absorption combined with extremely high chemical stability of both components. In this paper we discuss in detail the structural, optical and photoelectrochemical properties of the hybrids. We particularly focus on the nature of electronic interaction between the organic (polyheptazine) and inorganic (TiO_2) components, the knowledge of which is a fundamental prerequisite for optimizing and tuning of these materials.

Experimental and theoretical methods

For synthesis of TiO_2–polyheptazine hybrids a commercial TiO_2 powder (Hombikat UV 100, Sachtleben, Germany, anatase, specific surface area (BET) $\sim$300 m^2 g^{-1}, crystallite size $<$ 10 nm) was used as a starting material. In order to modify the surface of TiO_2 with polyheptazine, we used a procedure described previously.[40] In short, the TiO_2 powder was placed in a Schlenk tube connected *via* an adapter with a round bottomed flask containing 1 g of urea, and heated in a muffle oven for 30 minutes at 400 °C. Pristine polyheptazine powder was prepared by heating melamine at 500 °C for two hours.[51–57] Hybrids with a polyheptazine core and TiO_2 shell were synthesized by impregnating polyheptazine powder in a solution prepared from 170 ml of isopropanol, 0.4 ml of HCl (conc.) and 15 ml of titanium tetraisopropoxide (Acros, 98%), followed by hydrolysis and calcination in air at 450 °C for 30 minutes and under vacuum (0.2 mbar) at 500 °C for 1 hour. Control samples containing SiO_2 instead of TiO_2 were prepared analogously using ethanolic solution of tetraethyl orthosilicate (Aldrich).

For photocurrent measurements electrodes consisting of a porous nanocrystalline film pressed onto an ITO-glass were prepared. The conducting ITO-glass substrate (Präzision Glas & Optik, Germany, sheet resistance of $\sim$10 Ω sq^{-1}) was first cut into 2.5 $\times$ 1.5 cm pieces and then subsequently degreased by sonicating in acetone and boiling NaOH (0.1 M), rinsed with demineralized water, and blown dry in a nitrogen stream. A suspension of 200 mg of TiO_2 in 1 ml of ethanol was sonicated for 10 minutes and then deposited onto the ITO glass by doctor blading using a scotch tape as frame and spacer. The electrodes were then dried at 100 °C, covered with a glass plate, pressed for 3 minutes at a pressure of 200 kg cm^{-2}, and heated in air at 450 °C for 30 minutes in order to ensure good electrical contact. This procedure yields an $\sim$2.5 μm thick layer of TiO_2 with excellent mechanical stability. Subsequently, the TiO_2 electrodes were modified with polyheptazine by the procedure described above. The photoelectrodes from other materials were prepared by doctor-blading a suspension in ethanol onto an ITO-glass. During photocurrent measurements the electrodes were pressed against an O-ring of an electrochemical cell leaving an irradiated area of 0.64 cm^2. The electrodes were irradiated from the backside (through the ITO glass) either by a 150 W Xenon lamp (Lot-Oriel), or, for wavelength-resolved measurements, using a tunable monochromatic light source provided with a 1000 W Xenon lamp and a universal grating monochromator Multimode 4 (AMKO, Tornesch, Germany) with a bandwidth of 10 nm. The electrochemical setup consisted of a BAS Epsilon Electrochemistry potentiostat and a three-electrode cell using a platinum counter electrode and a Ag/AgCl (3 M KCl) reference electrode.

Oxygen evolution was measured in a phosphate buffer (pH 7) by an OxySense 325i oxygen analyzer in a two-compartment cell under visible light (cut-off filter $\lambda > 420$ nm) irradiation from a 150 W Xenon lamp (Lot-Oriel). The irradiated electrode area was 0.5 cm^2, and the volume of the anode compartment was 5 ml. Iridium oxide nanoparticles were deposited onto the hybrid electrode by the method described by Maeda *et al*.[60]

Optical absorption properties of all samples were determined using a Kubelka–Munk function $F(R_\infty)$[61–63] that can be obtained from diffuse reflectance data[64,65] as $F(R_\infty) = (1 - R_\infty)^2/2R_\infty$, where R_∞ is diffuse reflectance of the sample relative to the reflectance of a standard. UV/Vis diffuse reflectance spectra were obtained relative to the reflectance of a standard ($BaSO_4$) using a Shimadzu UV-2401 UV/Vis recording spectrophotometer equipped with a diffuse reflectance accessory. The samples were pressed pellets of a mixture of 2 g of $BaSO_4$ with 50 mg of the powder. X-Ray diffraction measurements were performed with a Philips X'Pert PW 3040/60 diffractometer. FTIR measurements were performed using a Jasco FT-IR FT/IR-4100 spectrometer. The photoluminescence signal was dispersed by a spectrograph (ARC-SpectraPro 300i) with a spectral bandpass $<$2.5 nm and detected by a gatable intensified CCD (PI MAX Princeton Inst.) The laser excitation energy was 330 nm and the power density was 25 mW cm^{-2}.

The QC calculations were performed by a semiempirical method MSNDDO (Modified Symmetrized Neglect of Diatomic Differential Overlap) using self-developed QCH software. QCH is a version of QuChem program,[66,67] using integral calculation, Fockian formation, diagonalization, SCF, energy evaluation, calculation of full energy derivatives in the Cartesian coordinates and of dipole moments modules taken from MSINDO program,[68–70] kindly provided by the developers. Geometry optimization, transformation of energy derivatives from the Cartesian to internal coordinates, calculation of vibrational spectra and IR-spectra intensities, as well as file system and restart modules, are taken from original QuChem program. The method is parameterized to reproduce the spatial structure and electronic properties of "reference" molecules. Complete space structure optimization and evaluation of enthalpy of formation ($\Delta_f H$) have been performed in a cluster (supermolecular) approach for each cluster. The restricted Hartree–Fock (RHF) method has been applied in the present study for a close-shell singlet (^1S) state calculation.

Results and discussion

Structural properties

The FTIR spectrum of polyheptazine displays a typical fingerprint of polyheptazine-type materials known from the literature (Fig. 3).[51,52,71–73]

Broad absorption bands corresponding to the NH stretching vibrations are observed between 3350 and 3150 cm^{-1}, and

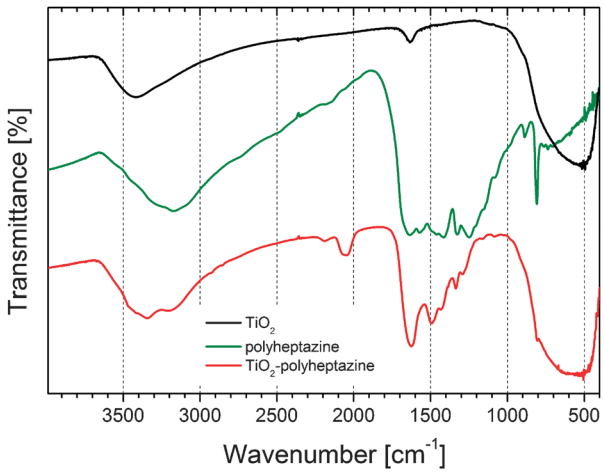

Fig. 3 FTIR spectra (KBr pellet) of TiO_2, polyheptazine, and TiO_2–polyheptazine hybrid. The spectra are offset for clarity.

manifold peaks arising from C=N and C–N vibrations are found between 1700 and 1100 cm^{-1}. The sharp peaks at 808 cm^{-1} and 887 cm^{-1} are typical for out-of-plane breathing modes of triazine/heptazine rings.[51,52,71–73] The FTIR spectrum of the TiO_2–polyheptazine hybrid is practically a sum of the IR spectra of the TiO_2 and polyheptazine components, plus the stretching C≡N vibrations at 2200–2050 cm^{-1} suggesting the presence of cyanamide and/or dicyandiamide traces.[74–76] The polyheptazine layer at the surface of TiO_2 nanocrystallites is presumably very thin so that the XRD spectrum of the hybrid material shows only anatase peaks (see ESI†, Fig. S2). In the Raman spectrum of the TiO_2–polyheptazine hybrid, however, the wide band of polyheptazine is clearly distinguishable (see ESI†, Fig. S3).

Understanding the nature of the interaction between TiO_2 and polyheptazine is critically important for the assessment of their electronic coupling. Mitoraj *et al.* proposed a secondary amine linkage (–NH–) formed upon condensation reaction between the amino group of polyheptazine and the surface hydroxyl group of TiO_2.[42,43] Drawing on this suggestion, we have performed quantum chemical simulations of polyheptazine's grafting onto the [100] surface of anatase using the semiempirical method MSNDDO. The linear dimensions of the used Ti54H cluster (represented as $Ti_{54}O_{98}(OH)_{48}(H_2O)_4$ and being analogous to that described previously by Homann *et al.*)[77] are 20.1 × 7.2 × 7.5 Å, making it sufficiently large to represent the real surface of commonly used TiO_2 particles. Polyheptazine was simulated by a cluster PH5 consisting of five heptazine fragments connected *via* bridging N atoms in a truncated triangle fashion. Unsaturated valences on the edges of the cluster are compensated by H atoms, giving four terminal NH_2-groups and four bridging NH-groups. The structure of the PH5 cluster is buckled in agreement with the literature results.[78] The distance between two amino-N atoms, potentially available for grafting on a flat surface, is 8.67 Å. However, the cluster is very flexible. For instance, deformation by 2 Å in both directions from the equilibrium leads to only 4–6 kcal mol^{-1} increase in energy (see ESI†, Fig. S4). One can discriminate two flat areas on the [100] surface of the Ti54H cluster, divided by a "trench". Consequently, a PH5 sheet can be grafted on the [100] surface of anatase TiO_2 in two principally

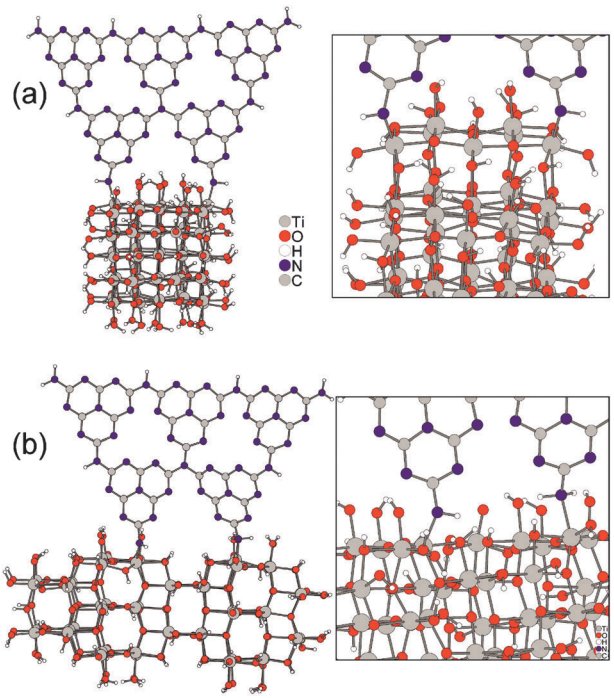

Fig. 4 Two possible modi of polyheptazine grafting onto the [100] anatase surface from semiempirical MSNDDO simulations: (a) Ti54M1; (b) Ti54M2 cluster.

different manners, namely occupying sites on one "island" (Ti54M1 cluster, Fig. 4a) or "bridging" two isles over the "trench" (Ti54M2 cluster, Fig. 4b).

Notably, we found that (i) the PH5 conformation is sensitive to the mode of chemical bonding to the surface of TiO_2 and can alter, compensating energetic penalties due to electronic effects of non-optimal bond type; (ii) a proton-transfer process may occur on the interface between the hydrogen-rich TiO_2 surface and PH5. Thus, for example, both Ti54M1 and Ti54M2 modi initially had two Ti–N(H)–C linkages, but in Ti54M2 one of bridges spontaneously deprotonated the neighbouring OH-group, forming a coordination C–NH_2···Ti fragment, while in Ti54M1 the both –NH– linkages are preserved. Similarly, in Ti54M1 the surface hydroxyl proton could be spontaneously transferred to the alpha-position of heptazine, leading to the Ti54M1-H-amide system (see ESI†, Fig. S5). The conclusions from our simulations are obviously limited by assuming the [100] anatase surface, whereby the real surface structure might be non-flat, dehydroxylated and/or amorphous due to the harsh conditions during the urea pyrolysis treatment. However, it can be established that the main factor of the binding stability is the coincidence between the N–N distances in polyheptazine and Ti–Ti on the TiO_2 surface, and that the inherent flexibility of polyheptazine sheets plays an important role for the hybrid's stability.

Optical and photoelectrochemical properties

In order to understand the photoactivity of TiO_2–polyheptazine hybrids, we first investigated the properties of the polyheptazine component alone. Polyheptazine powder exhibits excellent thermal stability with significant weight loss occurring first above 550 °C upon heating in air (see ESI†, Fig. S6). The yellowish material

 This journal is © the Owner Societies 2011

shows a steep increase in optical absorption in the near visible (Fig. 5a) with a direct optical bandgap of 2.90 eV (Fig. 5b), corresponding to a wavelength of 428 nm. In order to further probe the electronic properties of polyheptazine, cyclic voltammetry was employed (Fig. 5c). The cyclic voltammogram shows irreversible oxidation and reduction waves separated by *ca.* 2.3 V. Assuming that the oxidation and reduction potentials of a polymeric material can typically be correlated with the potentials of its HOMO (valence band) and LUMO (conduction band), respectively, the electrochemical bandgap of polyheptazine seems to be slightly lower than the optical one. More importantly, the photocurrent response of pure polyheptazine was found to be very poor (Fig. 5d). Even with a full light of a 150 W Xenon lamp ($\lambda > 320$ nm) only small photocurrents (~ 1 μA cm^{-2}) are detectable. Interestingly, the photocurrent direction switches from anodic to cathodic at a potential of *ca.* +0.25 V *vs.* NHE. Such photocurrent response is evocative of bulk photoeffects in insulating materials with very low charge carrier mobility.[79]

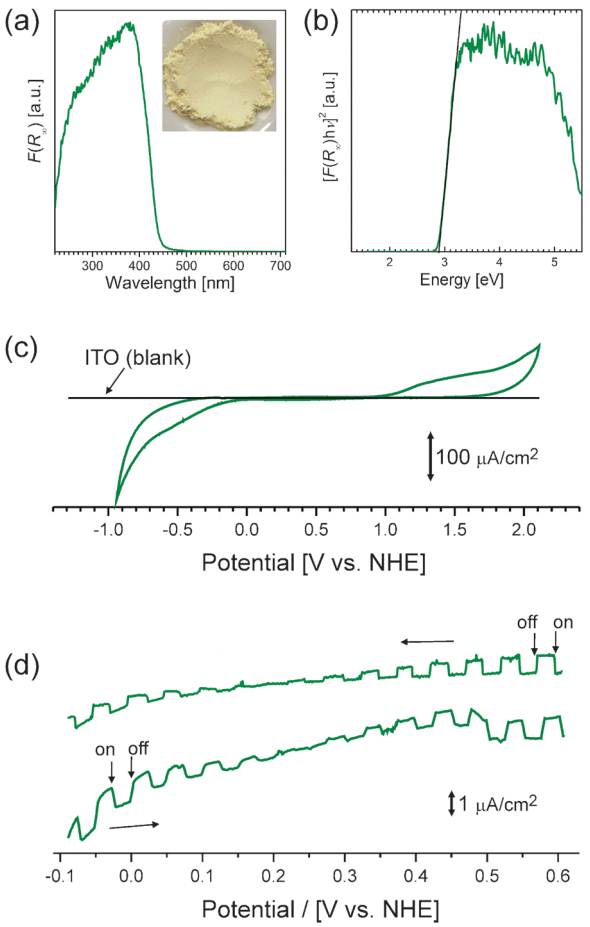

Fig. 5 (a) Photograph of polyheptazine and a corresponding plot of Kubelka–Munk function *vs.* wavelength measured by diffuse reflectance spectroscopy; (b) bandgap determination using a $[F(R_\infty)h\nu]^2$ *vs.* $h\nu$ plot (assuming direct optical transition) of polyheptazine; (c) cyclic voltammogram of polyheptazine powder deposited on ITO recorded in the dark in an acetonitrile solution of tetrabutylammonium hexafluorophosphate ($TBAPF_6$, 0.1 M) at a sweep rate of 50 mV s^{-1}; (d) photocurrents measured under intermittent irradiation from a 150 W Xenon lamp (cut-off filter 320 nm) during cathodic and anodic potential scans (5 mV s^{-1}) in acetonitrile + $TBAPF_6$ (0.1 M).

In other words, the behavior of pristine polyheptazine can be best understood as that of a "low-bandgap insulator", or of a "wide-bandgap intrinsic semiconductor" with very low charge mobility, whereby its Fermi level is in the middle of the bandgap and coincides with the photocurrent switching potential (+0.25 V *vs.* NHE).

A very different behaviour is observed in the case of the TiO_2–polyheptazine *hybrid* electrodes (Fig. 2a) consisting of a porous layer of TiO_2 powder pressed onto an ITO-glass and modified at the surface with polyheptazine. The raw photocurrent spectrum (Fig. 6a) shows a significant anodic response down to ~ 700 nm. In contrast, the photocurrents at pure (unmodified) TiO_2 electrodes vanish at wavelengths above 400 nm.[39–41] The spike-like shape of photocurrent transients is indicative of surface recombination processes going on.[80–84] After the initial rise of photocurrent upon switching-on the light, a rapid decay is observed, which can be ascribed to accumulation of photogenerated holes in the surface polyheptazine layer, which, in turn, renders their recombination with photogenerated electrons more likely. However, more importantly, under continuous *visible* light ($\lambda > 455$ nm) irradiation (Fig. 6b) the photocurrent levels off at a stable value, which suggests that a significant portion of accumulated photogenerated holes can escape recombination and induce water oxidation. Indeed, after deposition of IrO_2 nanoparticles as a co-catalyst, dioxygen was detected as the product of water oxidation under visible light ($\lambda > 420$ nm) irradiation, confirming thus the water-splitting ability of our hybrid photoelectrodes (Fig. 7). Optimization studies and long-term stability investigation

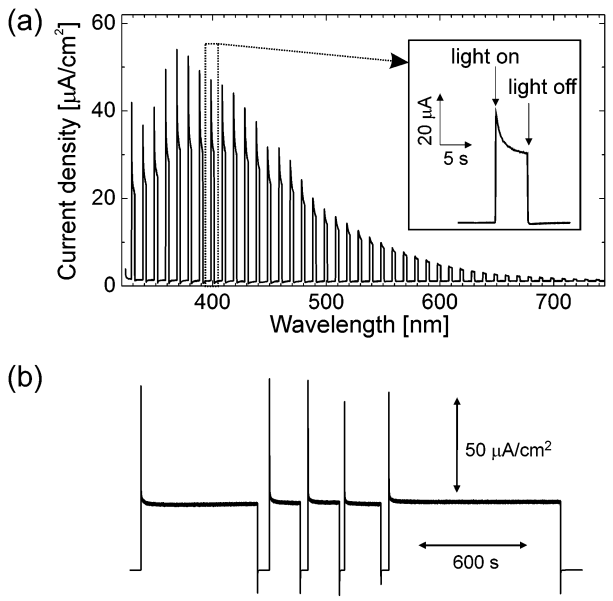

Fig. 6 (a) Photocurrent response of an ITO-glass electrode covered with a layer (thickness ~ 2.5 μm) nanocrystalline TiO_2 surface-modified with polyheptazine (see Fig. 2a) as a function of the irradiation wavelength (without correction for the change of light intensity) under intermittent light irradiation in $LiClO_4$ (0.1 M) at 0.5 V *vs.* Ag/AgCl (3 M). The inset shows the photocurrent transient at $\lambda = 400$ nm. (b) The same electrode under intermittent *visible* light ($\lambda > 455$ nm) irradiation from a 150 W Xenon lamp measured in a phosphate buffer (0.1 M) at 0.5 V *vs.* Ag/AgCl (3 M).

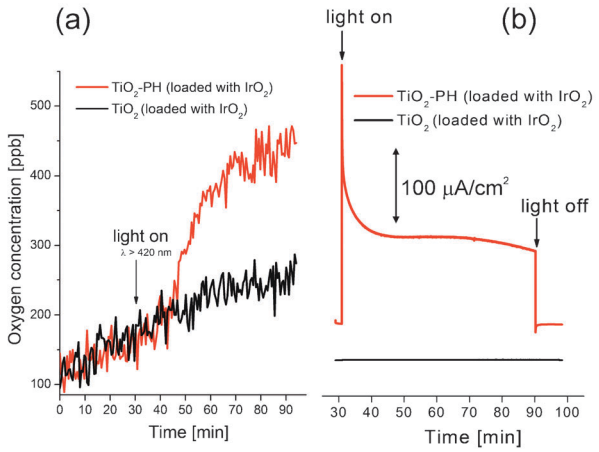

Fig. 7 Oxygen concentration (a) and photocurrent (b) measured under visible light (cut-off filter $\lambda > 420$ nm) irradiation in a phosphate buffer (0.1 M; pH 7) at 0.5 V *vs.* Ag/AgCl for TiO_2–PH and pristine TiO_2 photoelectrodes modified with IrO_2 nanoparticles. The irradiated electrode area was 0.5 cm^2, and the volume of the anode compartment was 5 ml. As expected, pristine TiO_2 photoelectrode modified with IrO_2 nanoparticles shows only negligible photocurrents and does not show any oxygen evolution under visible light irradiation.

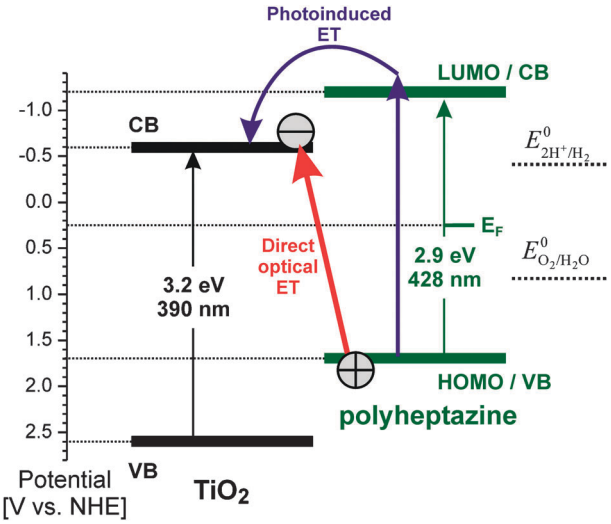

Fig. 8 Potential diagram of the TiO_2–polyheptazine interface (pH 7). The positions of the TiO_2 band edges are taken from the literature.[40,100] For polyheptazine the HOMO (valence band) and LUMO (conduction band) positions were postulated assuming that polyheptazine is an intrinsic semiconductor having its Fermi level positioned in the middle of the bandgap at +0.25 V *vs.* NHE (see Fig. 5d). Two possible photoexcitation pathways are indicated: *photoinduced electron transfer* (*blue*) initiated, upon absorption of a photon, by promotion of an electron from the ground state into the excited state of polyheptazine, followed by electron injection into the conduction band of TiO_2; *direct optical electron transfer* (*red*) from the polyheptazine HOMO (valence band) into the TiO_2 conduction band.

are currently underway. However, we note that the remarkable stability of photocurrents reported here is in stark contrast to relatively fast and continuous photocurrent decay typically observed on photoanodes undergoing fast photodegradation processes.[85]

Based on these results a scheme depicting the electronic structure of the TiO_2–polyheptazine interface can be constructed (Fig. 8). The strong visible-light photocurrent response of the hybrid electrode (Fig. 6) is evidently due to efficient photosensitization of TiO_2 by polyheptazine. In general, there are two different possible photosensitization mechanisms at the TiO_2–chromophore interface, depending mainly on the electronic coupling between TiO_2 and the chromophore (Fig. 8).[86–89]

In case of a weak coupling, the so-called *photoinduced electron transfer* occurs in which an absorbed photon promotes an electron from the chromophore's ground state into an excited state, followed by a very fast electron injection from the excited state into the conduction band of TiO_2. This mechanism is typical, for example, for nanocrystalline TiO_2 sensitized with ruthenium dyes known from the Grätzel-type solar cells.[90] Additionally, the so-called *direct optical electron transfer* from the chromophore's HOMO into the conduction band of TiO_2 can occur in case of a strong coupling. Such a process involves a single electronic state (charge transfer state) and is known to occur, for example, at TiO_2 covalently sensitized with ferrocyanide ion,[91–93] catechol,[87–88,94] dopamine,[95] or chlorophenols.[96,97]

Typically, the direct optical charge transfer is revealed by an additional optical absorption band at energies lower than the absorption edge of either component. In other words, the optical absorption spectrum of a hybrid material is not a simple sum of the absorption spectra of individual components. Obviously, the fact that the photocurrent response of a TiO_2–polyheptazine hybrid electrode extends well beyond (down to ~700 nm) the absorption edge of both polyheptazine (430 nm) and TiO_2 (390 nm) immediately suggests that an interfacial charge-transfer complex might be formed between polyheptazine (donor) and TiO_2 (acceptor). The most straightforward way to identify the new absorption feature arising from the interfacial charge-transfer is a differential analysis of normalized absorption spectra.[98,99]

Fig. 9 shows the normalized spectra of TiO_2 (a), polyheptazine (b), and the TiO_2–polyheptazine hybrid (c). The differential absorption spectrum (d) was obtained by subtracting the spectra of the components (TiO_2 and polyheptazine) from the spectrum of the hybrid. It is ascribed to the charge-transfer band arising from the direct optical electron transfer from the HOMO of polyheptazine into the conduction band of TiO_2.

Its low-energy shoulder can be extrapolated to ~2.3 eV, corresponding exactly to the energy difference between the HOMO of polyheptazine (+1.7 V *vs.* NHE) and the conduction band edge of TiO_2 (−0.6 V *vs.* NHE) (see Fig. 7).

It is well known that the absorption edge of polymers can shift to lower energies after structural changes leading to enhanced conjugation. This has been very recently reported also for polyheptazine-like carbon nitride powders.[48] In order to rule out the possibility that the new absorption feature in the hybrid is simply due to any structural change of the polyheptazine component alone, we performed control experiments in which we impregnated pristine polyheptazine powder with TiO_2 by treating it with a titanium tetraisopropoxide solution. The TiO_2 layer at the surface was very thin so that only polyheptazine peaks were revealed in the XRD spectra (see ESI†, Fig. S7). The polyheptazine–TiO_2 hybrid revealed the same differential absorption feature at ~2.3 eV (Fig. 10a)

This journal is © the Owner Societies 2011

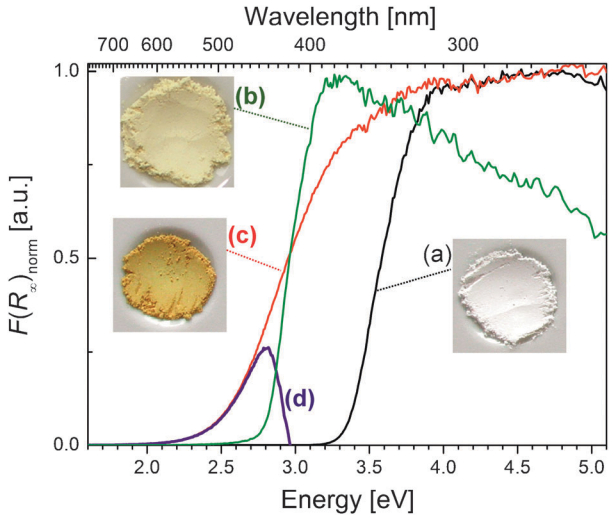

Fig. 9 Colors and corresponding *normalized* absorption spectra (Kubelka–Munk functions) of TiO_2 (a), polyheptazine (b) and TiO_2–polyheptazine hybrid (c). The blue curve (d) is a differential spectrum obtained by subtraction: (d) = (c) − (a) − (b). It is noted that the negative values of the differential spectrum at energies above 3.0 eV are an artefact due to normalization.

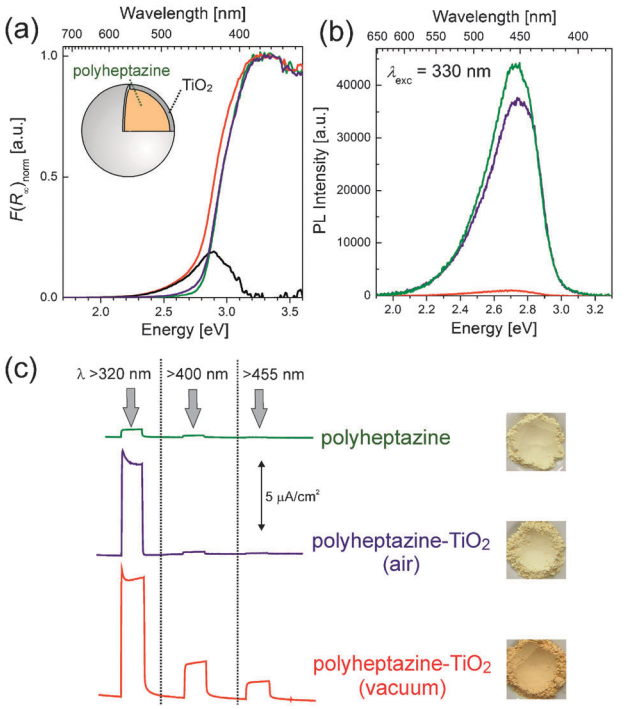

Fig. 10 Control experiments with polyheptazine powder impregnated with small amounts of TiO_2. (a) Normalized absorption spectra of polyheptazine (*green*), polyheptazine impregnated by TiO_2 after heating in air at 450 °C (*blue*), and after additional heat treatment under vacuum (0.2 mbar) at 500 °C (*red*); the black line is the differential spectrum obtained by subtraction of polyheptazine (*green*) from the polyheptazine–TiO_2 (vacuum, *red*) spectrum. (b) Photoluminescence spectra of polyheptazine (*green*), polyheptazine–TiO_2 (air, *blue*), and polyheptazine–TiO_2 (vacuum, *red*). (c) Photocurrent response of TiO_2-impregnated samples measured in $LiClO_4$ (0.1 M) at 0.5 V *vs.* Ag/AgCl under intermittent irradiation from a 150 W Xenon lamp with cut-off filters 320 nm, 400 nm, and 455 nm.

as in the case of TiO_2–polyheptazine hybrids. Interestingly, during the synthesis of this control material, after calcination in air at 450 °C the sample did not change color significantly. Only after an additional heat treatment under vacuum at 500 °C the absorption edge shifted down, We conclude that, in this case, the second heating step was necessary to form a chemical bond between TiO_2 and polyheptazine by condensation reaction of surface OH-groups in TiO_2 and NH_2-group of polyheptazine.

In the case of TiO_2–polyheptazine hybrids with TiO_2 core described above, this step is not necessary since the bond between TiO_2 and polyheptazine is established during the modification procedure under the atmosphere of urea pyrolysis products. It is suggested that defective and/or dehydroxylated surface of TiO_2 is necessary for the hybrid formation. More importantly, in comparison to pristine polyheptazine and the impregnated sample heated only in air which exhibit strong photoluminescence, the photoluminescence efficiency in the vacuum-treated sample is drastically reduced (Fig. 10b). This represents an additional evidence for the charge-transfer process to the TiO_2 shell leading to intense quenching of photoluminescence. Furthermore, the normalized PL spectra revealed a slight red shift for the vacuum-treated sample (see ESI†, Fig. S8). Finally, as expected, only the vacuum-heat-treated samples exhibited photocurrents under *visible* ($\lambda > 400$ nm) light (Fig. 10c).

Here it should be also noted that treating simply the pristine polyheptazine under vacuum at 500 °C did not lead to any changes in optical absorption (see ESI†, Fig. S9). Similarly, the analysis of differential absorption spectra did not reveal any low-energy absorption feature when TiO_2 was replaced by large-bandgap insulating SiO_2 (see ESI†, Fig. S10). We also exclude the possibility that the low energy feature could be solely due to the formation of Ti^{3+} defects in our materials. In contrast, the Ti 2p XP spectra of the hybrids show binding energies and Ti 2p doublet peak separations (5.6–5.7 eV) typical for Ti^{4+}, as in TiO_2 (see ESI†, Fig. S11).[101–105]

The low-energy light absorption and photocurrent response is thus evidently the consequence of formation of a charge transfer complex between polyheptazine and semiconducting TiO_2. The mechanism of photocurrent generation can be summarized as follows (see Fig. 8). The photoholes in the polyheptazine layer are, from the thermodynamic point of view, positive enough (+1.7 V *vs.* NHE; pH 7) to allow for water oxidation (+0.82 V *vs.* NHE; pH 7). The photogenerated electrons are assumed to be energetically at the conduction band edge of TiO_2 having a potential more negative (−0.6 V *vs.* NHE; pH 7) than the reduction potential of protons (−0.41 V *vs.* NHE; pH 7). The photocurrent onset potential is slightly more positive (−0.45 V *vs.* NHE), which is attributed to enhanced recombination at potentials near the conduction band edge of TiO_2 (see ESI†, Fig. S12).

Conclusions

We have shown that the visible-light photoactivity of TiO_2–polyheptazine hybrid materials is governed by the charge-transfer complex formed between polyheptazine (donor) and TiO_2 (acceptor). The direct optical electron transfer allows for photon harvesting at energies lower than the bandgap of either TiO_2 or polyheptazine. In other words, these materials are

not mere *composites*, that simply sum up the individual properties of the components, but genuine *hybrids* exhibiting new features emerging due to the mutual interaction of their building blocks.[106] Notably, the resulting energetic positions of photogenerated charges allow for feasibility of water oxidation by holes at the polyheptazine layer, while still keeping the advantage of generating reactive electrons at a relatively negative conduction band edge of TiO_2. The ability of these hybrid photoelectrodes to induce visible light-driven water-splitting was confirmed by observation of dioxygen production on photoelectrodes modified with IrO_2 nanoparticles acting as a co-catalyst. The quantum-chemical simulations demonstrate that the interface between the hydrated/hydroxylated TiO_2 surface and the polyheptazine moiety is a complex system, where proton-transfer processes are feasible. The latter might assist water oxidation processes which are known to require proton-coupled electron transfers. Importantly, it has been recently shown that the electron–hole recombination is the key loss process limiting water photooxidation at nanocrystalline TiO_2 and Fe_2O_3 photoanodes.[107,108] In this context, hybrid architectures consisting of a metal oxide electron collector coupled with a robust metal-free organic sensitizer appear highly interesting since they enable direct photogeneration of charges that are spatially separated between two phases with different electronic properties, without compromising the stability. In order to improve photooxidation efficiency, one of the key challenges seems to be the improvement of coupling of hybrid materials with efficient oxygen evolving co-catalysts.[25,109–115] Since metal oxides different from TiO_2 may be possibly utilized and the electronic properties of polyheptazine materials can be tuned by doping,[116–118] our findings also open up a route for synthesis of further novel photoactive hybrid materials. Such hybrid materials may also find applications beyond the scope of solar water splitting in a broader research area of solar cells and other photo-responsive devices.

Acknowledgements

We acknowledge the financial support by the MIWFT-NRW. We thank Prof. Thomas Bredow (Bonn University) for kindly granting MSINDO code, Prof. Laurie Peter for valuable discussions, Dr Jesus Rodriguez Ruiz and Andreas Kunzmann for their contributions to this work, Armin Lindner for his help with the design of the oxygen detection reactor, Prof. Hans-Peter Steinrück and Dr Florian Maier for providing experimental facilities at PC II, Prof. Karsten Meyer for providing lab space at ACII in Erlangen, and Sachtleben Chemie for providing Hombikat UV 100. The support of the Center for Electrochemical Sciences (CES) is gratefully acknowledged.

Notes and references

1 J. A. Turner, *Science*, 2004, **305**, 972–974.
2 N. S. Lewis and D. G. Nocera, *Proc. Natl. Acad. Sci. U. S. A.*, 2006, **103**, 15729–15735.
3 V. Balzani, A. Credi and M. Venturi, *ChemSusChem*, 2008, **1**, 26–58.
4 R. Memming, *Semiconductor Electrochemistry*, Wiley-VCH, Weinheim, 2001.
5 K. Rajeshwar, *J. Appl. Electrochem.*, 2007, **37**, 765–787.
6 K. Maeda, T. Takata, M. Hara, N. Saito, Y. Inoue, H. Kobayashi and K. Domen, *J. Am. Chem. Soc.*, 2005, **127**, 8286–8287.
7 A. Kudo and Y. Miseki, *Chem. Soc. Rev.*, 2009, **38**, 253–278.
8 K. Maeda, A. Xiong, T. Yoshinaga, T. Ikeda, N. Sakamoto, T. Hisatomi, M. Takashima, D. Lu, M. Kanehara, T. Setoyama, T. Teranishi and K. Domen, *Angew. Chem., Int. Ed.*, 2010, **49**, 4096–4099, S4096/4091-S4096/4094.
9 K. Maeda and K. Domen, *J. Phys. Chem. Lett.*, 2010, **1**, 2655–2661.
10 O. Khaselev and J. A. Turner, *Science*, 1998, **280**, 425–427.
11 A. B. Murphy, P. R. F. Barnes, L. K. Randeniya, I. C. Plumb, I. E. Grey, M. D. Horne and J. A. Glasscock, *Int. J. Hydrogen Energy*, 2006, **31**, 1999–2017.
12 R. van de Krol, Y. Liang and J. Schoonman, *J. Mater. Chem.*, 2008, **18**, 2311–2320.
13 H. Dau, C. Limberg, T. Reier, M. Risch, S. Roggan and P. Strasser, *ChemCatChem*, 2010, **2**, 724–761.
14 R. Eisenberg and H. B. Gray, *Inorg. Chem.*, 2008, **47**, 1697–1699.
15 T. A. Betley, Q. Wu, T. Van Voorhis and D. G. Nocera, *Inorg. Chem.*, 2008, **47**, 1849–1861.
16 J. Tang, J. R. Durrant and D. R. Klug, *J. Am. Chem. Soc.*, 2008, **130**, 13885–13891.
17 A. Imanishi, T. Okamura, N. Ohashi, R. Nakamura and Y. Nakato, *J. Am. Chem. Soc.*, 2007, **129**, 11569–11578.
18 A. Valdés, Z. W. Qu, G. J. Kroes, J. Rossmeisl and J. K. Nørskov, *J. Phys. Chem. C*, 2008, **112**, 9872–9879.
19 B. D. Alexander, P. J. Kulesza, I. Rutkowska, R. Solarska and J. Augustynski, *J. Mater. Chem.*, 2008, **18**, 2298–2303.
20 A. Fujishima and K. Honda, *Nature*, 1972, **238**, 37–38.
21 H. H. Kung, H. S. Jarrett, A. W. Sleight and A. Ferretti, *J. Appl. Phys.*, 1977, **48**, 2463–2469.
22 M. A. Butler, *J. Appl. Phys.*, 1977, **48**, 1914–1920.
23 D. E. Scaife, *Sol. Energy*, 1980, **25**, 41–54.
24 C. J. Sartoretti, B. D. Alexander, R. Solarska, I. A. Rutkowska, J. Augustynski and R. Cerny, *J. Phys. Chem. B*, 2005, **109**, 13685–13692.
25 A. Kay, I. Cesar and M. Grätzel, *J. Am. Chem. Soc.*, 2006, **128**, 15714–15721.
26 B. Yang, Y. Zhang, E. Drabarek, P. R. F. Barnes and V. Luca, *Chem. Mater.*, 2007, **19**, 5664–5672.
27 I. Cesar, K. Sivula, A. Kay, R. Zboril and M. Gratzel, *J. Phys. Chem. C*, 2008, **113**, 772–782.
28 R. Solarska, A. Królikowska and J. Augustyński, *Angew. Chem., Int. Ed.*, 2010, **49**, 7980–7983.
29 K. G. Upul Wijayantha, S. Saremi-Yarahmadi and L. M. Peter, *Phys. Chem. Chem. Phys.*, 2011, **13**, 5264–5270.
30 M. Grätzel, *Nature*, 2001, **414**, 338–344.
31 F. E. Osterloh, *Chem. Mater.*, 2008, **20**, 35–54.
32 R. Solarska, A. Królikowska and J. Augustyński, *Angew. Chem., Int. Ed.*, 2010, **49**, 7980–7983.
33 A. Iwase and A. Kudo, *J. Mater. Chem.*, 2010, **20**, 7536–7542.
34 S. H. Baeck, T. F. Jaramillo, C. Braendli and E. W. McFarland, *J. Comb. Chem.*, 2002, **4**, 563–568.
35 M. Woodhouse, G. S. Herman and B. A. Parkinson, *Chem. Mater.*, 2005, **17**, 4318–4324.
36 M. Woodhouse and B. A. Parkinson, *Chem. Soc. Rev.*, 2009, **38**, 197–210.
37 J. E. Katz, T. R. Gingrich, E. A. Santori and N. S. Lewis, *Energy Environ. Sci.*, 2009, **2**, 103–112.
38 W. J. Youngblood, S.-H. A. Lee, Y. Kobayashi, E. A. Hernandez-Pagan, P. G. Hoertz, T. A. Moore, A. L. Moore, D. Gust and T. E. Mallouk, *J. Am. Chem. Soc.*, 2009, **131**, 926–927.
39 R. Beranek and H. Kisch, *Electrochem. Commun.*, 2007, **9**, 761–766.
40 R. Beranek and H. Kisch, *Photochem. Photobiol. Sci.*, 2008, **7**, 40–48.
41 R. Beranek, J. M. Macak, M. Gaertner, K. Meyer and P. Schmuki, *Electrochim. Acta*, 2009, **54**, 2640–2646.
42 D. Mitoraj and H. Kisch, *Angew. Chem., Int. Ed.*, 2008, **47**, 9975–9978.
43 D. Mitoraj and H. Kisch, *Chem.–Eur. J.*, 2010, **16**, 261.
44 J. Liebig, *Ann. Pharm.*, 1834, **10**, 1–47.
45 X. Wang, K. Maeda, A. Thomas, K. Takanabe, G. Xin, J. M. Carlsson, K. Domen and M. Antonietti, *Nat. Mater.*, 2009, **8**, 76–80.
46 X. Wang, K. Maeda, X. Chen, K. Takanabe, K. Domen, Y. Hou, X. Fu and M. Antonietti, *J. Am. Chem. Soc.*, 2009, **131**, 1680–1681.

 This journal is © the Owner Societies 2011

47 X. Chen, J. Zhang, X. Fu, M. Antonietti and X. Wang, *J. Am. Chem. Soc.*, 2009, **131**, 11658–11659.
48 J. Zhang, X. Chen, K. Takanabe, K. Maeda, K. Domen, J. D. Epping, X. Fu, M. Antonietti and X. Wang, *Angew. Chem., Int. Ed.*, 2010, **49**, 441–444, S441/441-S441/444.
49 A. Schmidt, *Chem. Ing. Tech.*, 1966, **38**, 1140–1144.
50 A. Schmidt, *Monatsh. Chem.*, 1968, **99**, 664–671.
51 B. Juergens, E. Irran, J. Senker, P. Kroll, H. Mueller and W. Schnick, *J. Am. Chem. Soc.*, 2003, **125**, 10288–10300.
52 B. V. Lotsch, M. Doeblinger, J. Sehnert, L. Seyfarth, J. Senker, O. Oeckler and W. Schnick, *Chem.–Eur. J.*, 2007, **13**, 4969–4980.
53 A. Sattler, S. Pagano, M. Zeuner, A. Zurawski, D. Gunzelmann, J. Senker, K. Mueller-Buschbaum and W. Schnick, *Chem.–Eur. J.*, 2009, **15**, 13161–13170, S13161/13161-S13161/13163.
54 Y. Zhao, D. Yu, H. Zhou, Y. Tian and O. Yanagisawa, *J. Mater. Sci.*, 2005, **40**, 2645–2647.
55 A. Thomas, A. Fischer, F. Goettmann, M. Antonietti, J.-O. Mueller, R. Schloegl and J. M. Carlsson, *J. Mater. Chem.*, 2008, **18**, 4893–4908.
56 B. V. Lotsch and W. Schnick, *Chem.–Eur. J.*, 2007, **13**, 4956–4968.
57 X. Li, J. Zhang, L. Shen, Y. Ma, W. Lei, Q. Cui and G. Zou, *Appl. Phys. A: Mater. Sci. Process.*, 2009, **94**, 387–392.
58 M. Doeblinger, B. V. Lotsch, J. Wack, J. Thun, J. Senker and W. Schnick, *Chem. Commun.*, 2009, 1541–1543.
59 L. Seyfarth, J. Seyfarth, B. V. Lotsch, W. Schnick and J. Senker, *Phys. Chem. Chem. Phys.*, 2010, **12**, 2227–2237.
60 K. Maeda, M. Higashi, B. Siritanaratkul, R. Abe and K. Domen, *J. Am. Chem. Soc.*, 2011, **133**, 12334–12337.
61 P. Kubelka and F. Munk, *Z. Tech. Phys.*, 1931, **12**, 593–601.
62 P. Kubelka, *J. Opt. Soc. Am.*, 1948, **38**, 448–457.
63 P. Kubelka, *J. Opt. Soc. Am.*, 1954, **44**, 330–335.
64 A. P. Finlayson, V. N. Tsaneva, L. Lyons, M. Clark and B. A. Glowacki, *Phys. Status Solidi A*, 2006, **203**, 327–335.
65 B. Ohtani, *Chem. Lett.*, 2008, **37**, 216–229.
66 V. Khavryutchenko, *Eurasian Chem.-Technol. J.*, 2004, **6**, 157–170.
67 A. V. Khavryutchenko, V. D. Khavryutchenko and Z. Naturforsch, *A: Phys. Sci.*, 2005, **60**, 41–46.
68 B. Ahlswede and K. Jug, *J. Comput. Chem.*, 1999, **20**, 563–571.
69 B. Ahlswede and K. Jug, *J. Comput. Chem.*, 1999, **20**, 572–578.
70 T. Bredow and K. Jug, *Theor. Chem. Acc.*, 2005, **113**, 1–14.
71 T. Komatsu, *Macromol. Chem. Phys.*, 2001, **202**, 19–25.
72 T. Komatsu, *J. Mater. Chem.*, 2001, **11**, 802–803.
73 B. V. Lotsch and W. Schnick, *Chem. Mater.*, 2006, **18**, 1891–1900.
74 M. Davies and W. J. Jones, *Trans. Faraday Soc.*, 1958, **54**, 1454–1463.
75 W. J. Jones and W. J. Orville-Thomas, *Trans. Faraday Soc.*, 1959, **55**, 193–202.
76 R. O. Carter, R. A. Dickie, J. W. Holubka and N. E. Lindsay, *Ind. Eng. Chem. Res.*, 1989, **28**, 48–51.
77 T. Homann, T. Bredow and K. Jug, *Surf. Sci.*, 2004, **555**, 135–144.
78 M. Deifallah, P. F. McMillan and F. Cora, *J. Phys. Chem. C*, 2008, **112**, 5447–5453.
79 M. Kalaji, L. Nyholm, L. M. Peter and A. J. Rudge, *J. Electroanal. Chem.*, 1991, **310**, 113–126.
80 L. M. Abrantes and L. M. Peter, *J. Electroanal. Chem.*, 1983, **150**, 593–601.
81 L. M. Peter, *Chem. Rev.*, 1990, **90**, 753–769.
82 D. Tafalla, P. Salvador and R. M. Benito, *J. Electrochem. Soc.*, 1990, **137**, 1810–1815.
83 P. Salvador, M. L. Garcia Gonzalez and F. Munoz, *J. Phys. Chem.*, 1992, **96**, 10349–10353.
84 A. Hagfeldt, H. Lindstroem, S. Soedergren and S.-E. Lindquist, *J. Electroanal. Chem.*, 1995, **381**, 39–46.
85 W. J. Youngblood, S.-H. A. Lee, K. Maeda and T. E. Mallouk, *Acc. Chem. Res.*, 2009, **42**, 1966–1973.
86 C. Creutz, B. S. Brunschwig and N. Sutin, *J. Phys. Chem. B*, 2005, **109**, 10251–10260.
87 C. Creutz, B. S. Brunschwig and N. Sutin, *J. Phys. Chem. B*, 2006, **110**, 25181–25190.
88 W. R. Duncan and O. V. Prezhdo, *Annu. Rev. Phys. Chem.*, 2007, **58**, 143–184.
89 W. Macyk, K. Szacilowski, G. Stochel, M. Buchalska, J. Kuncewicz and P. Labuz, *Coord. Chem. Rev.*, 2010, **254**, 2687–2701.
90 D. F. Watson and G. J. Meyer, *Annu. Rev. Phys. Chem.*, 2005, **56**, 119–156.
91 E. Vrachnou, N. Vlachopoulos and M. Grätzel, *J. Chem. Soc., Chem. Commun.*, 1987, 868–870.
92 M. Khoudiakov, A. R. Parise and B. S. Brunschwig, *J. Am. Chem. Soc.*, 2003, **125**, 4637–4642.
93 W. Macyk, G. Stochel and K. Szacilowski, *Chem.–Eur. J.*, 2007, **13**, 5676–5687.
94 L. G. C. Rego and V. S. Batista, *J. Am. Chem. Soc.*, 2003, **125**, 7989–7997.
95 G.-L. Wang, J.-J. Xu and H.-Y. Chen, *Biosens. Bioelectron.*, 2009, **24**, 2494–2498.
96 A. G. Agrios, K. A. Gray and E. Weitz, *Langmuir*, 2004, **20**, 5911–5917.
97 S. Kim and W. Choi, *J. Phys. Chem. B*, 2005, **109**, 5143–5149.
98 V. N. Kuznetsov and N. Serpone, *J. Phys. Chem. B*, 2006, **110**, 25203–25209.
99 V. N. Kuznetsov and N. Serpone, *J. Phys. Chem. C*, 2009, **113**, 15110–15123.
100 L. Kavan, M. Grätzel, S. E. Gilbert, C. Klemenz and H. J. Scheel, *J. Am. Chem. Soc.*, 1996, **118**, 6716–6723.
101 I. Bertóti, M. Mohai, J. L. Sullivan and S. O. Saied, *Appl. Surf. Sci.*, 1995, **84**, 357–371.
102 C. Viornery, Y. Chevolot, D. Léonard, B.-O. Aronsson, P. Péchy, H. J. Mathieu, P. Descouts and M. Grätzel, *Langmuir*, 2002, **18**, 2582–2589.
103 F. Zhang, Z. Zheng, Y. Chen, X. Liu, A. Chen and Z. Jiang, *J. Biomed. Mater. Res.*, 1998, **42**, 128–133.
104 J. L. Ong, C. W. Prince and L. C. Lucas, *J. Biomed. Mater. Res.*, 1995, **29**, 165–172.
105 D. V. Kilpadi, G. N. Raikar, J. Liu, J. E. Lemons, Y. Vohra and J. C. Gregory, *J. Biomed. Mater. Res.*, 1998, **40**, 646–659.
106 D. Eder, *Chem. Rev.*, 2010, **110**, 1348–1385.
107 A. J. Cowan, J. Tang, W. Leng, J. R. Durrant and D. R. Klug, *J. Phys. Chem. C*, 2010, **114**, 4208–4214.
108 S. R. Pendlebury, M. Barroso, A. J. Cowan, K. Sivula, J. Tang, M. Grätzel, D. Klug and J. R. Durrant, *Chem. Commun.*, 2011, **47**, 716–718.
109 M. W. Kanan and D. G. Nocera, *Science*, 2008, **321**, 1072–1075.
110 M. W. Kanan, J. Yano, Y. Surendranath, M. Dinca, V. K. Yachandra and D. G. Nocera, *J. Am. Chem. Soc.*, 2010, **132**, 13692–13701.
111 D. A. Lutterman, Y. Surendranath and D. G. Nocera, *J. Am. Chem. Soc.*, 2009, **131**, 3838–3839.
112 J. G. McAlpin, Y. Surendranath, M. Dinca, T. A. Stich, S. A. Stoian, W. H. Casey, D. G. Nocera and R. D. Britt, *J. Am. Chem. Soc.*, 2010, **132**, 6882–6883.
113 Y. Surendranath, M. Dinca and D. G. Nocera, *J. Am. Chem. Soc.*, 2009, **131**, 2615–2620.
114 Y. Surendranath, M. W. Kanan and D. G. Nocera, *J. Am. Chem. Soc.*, 2010, **132**, 16501–16509.
115 E. M. P. Steinmiller and K.-S. Choi, *Proc. Natl. Acad. Sci. U. S. A.*, 2009, **106**, 20633–20636, S20633/20631-S20633/20632.
116 X. Wang, X. Chen, A. Thomas, X. Fu and M. Antonietti, *Adv. Mater.*, 2009, **21**, 1609–1612.
117 Y. Zhang, T. Mori, J. Ye and M. Antonietti, *J. Am. Chem. Soc.*, 2010, **132**, 6294–6295.
118 S. C. Yan, Z. S. Li and Z. G. Zou, *Langmuir*, 2010, **26**, 3894–3901.